PNAS RESEARCH ARTICLE | PHYSIOLOGY

Balanced control of thermogenesis by nuclear receptor corepressors in brown adipose tissue

Hannah J. Richter[a,b], Amy K. Hauck[b,c], Kirill Batmanov[b,c], Shin-Ichi Inoue[b,c], Bethany N. So[b,c], Mindy Kim[b,c], Matthew J. Emmett[b,c], Ronald N. Cohen[d], and Mitchell A. Lazar[a,b,c,1]

Contributed by Mitchell A. Lazar; received March 25, 2022; accepted July 7, 2022; reviewed by Christopher Glass and Bert O'Malley

Brown adipose tissue (BAT) is a key thermogenic organ whose expression of uncoupling protein 1 (UCP1) and ability to maintain body temperature in response to acute cold exposure require histone deacetylase 3 (HDAC3). HDAC3 exists in tight association with nuclear receptor corepressors (NCoRs) NCoR1 and NCoR2 (also known as silencing mediator of retinoid and thyroid receptors [SMRT]), but the functions of NCoR1/2 in BAT have not been established. Here we report that as expected, genetic loss of NCoR1/2 in BAT (NCoR1/2 BAT-dKO) leads to loss of HDAC3 activity. In addition, HDAC3 is no longer bound at its physiological genomic sites in the absence of NCoR1/2, leading to a shared deregulation of BAT lipid metabolism between NCoR1/2 BAT-dKO and HDAC3 BAT-KO mice. Despite these commonalities, loss of NCoR1/2 in BAT does not phenocopy the cold sensitivity observed in HDAC3 BAT-KO, nor does loss of either corepressor alone. Instead, BAT lacking NCoR1/2 is inflamed, particularly with respect to the interleukin-17 axis that increases thermogenic capacity by enhancing innervation. Integration of BAT RNA sequencing and chromatin immunoprecipitation sequencing data revealed that NCoR1/2 directly regulate *Mmp9*, which integrates extracellular matrix remodeling and inflammation. These findings reveal pleiotropic functions of the NCoR/HDAC3 corepressor complex in BAT, such that HDAC3-independent suppression of BAT inflammation counterbalances stimulation of HDAC3 activity in the control of thermogenesis.

thermogenesis | corepressor | transcription | inflammation | brown adipose tissue

Significance

Brown adipose tissue (BAT) helps mammals survive in the cold by burning calories to produce heat and is a target for combating obesity. Heat production by BAT requires HDAC3, a transcriptional coregulator whose activity requires interaction with nuclear receptor corepressors (NCoRs). Here we report that surprisingly, BAT lacking NCoRs produces heat normally despite loss of HDAC3 activity by activating an inflammatory pathway that stimulates BAT via the sympathetic nervous system. These findings highlight the importance of understanding the pleiotropic physiological functions of transcriptional coregulator complexes.

Obesity is an ongoing metabolic health crisis that lacks simple and effective therapeutics (1, 2). One potential avenue for the treatment of obesity is the activation of calorie consumption by brown adipose tissue (BAT) (3, 4). BAT is a major thermogenic organ in mammals and known to be active in adult humans, especially in response to adrenergic cold stimulus (5, 6). BAT uses fuels such as glucose and lipids to produce heat via uncoupling protein 1 (UCP1), a mitochondrial membrane protein that releases the mitochondrial proton gradient independently of ATP production (7). UCP1-independent thermogenic mechanisms are also possible, coming from sources such as creatine and calcium metabolism (8). A less well-studied contribution to thermogenesis is inflammation of BAT itself (9).

Inflammation of white adipose tissue is implicated in obesity and related metabolic disease pathogenesis, with specific macrophage subpopulations and crown-like structures often associated with poor adipose health (10–12). For beige adipose, macrophages and inflammation are commonly linked to a reduction in thermogenic capacity with obesity, although mechanisms of macrophage-adipose communication are debated (13–16). More recently, γδT cells have been shown to positively affect BAT thermogenesis through cytokines interleukin-17A (IL-17A) and IL-17F (17, 18). However, the transcriptional underpinnings of this novel thermogenic pathway have yet to be uncovered.

Nuclear receptors regulate gene expression by recruitment of specific coactivator or corepressor complexes to affect nearby histone posttranslational modifications (19). These coregulators are targets of interest for a variety of diseases (20). One such corepressor complex is the nuclear receptor corepressor (NCoR)–histone deacetylase 3 (HDAC3) complex, of which HDAC3 is the enzymatic component (21). NCoR1 or NCoR2 (also known as silencing mediator of retinoid and thyroid receptor [SMRT]) is required to activate the deacetylase function of HDAC3 (22). Previous work has described the requirement of HDAC3 for acute thermogenic capacity in BAT, in part by deacetylating and activating peroxisome proliferator–activated receptor gamma coactivator 1-alpha (PGC1-α), which is a coactivator for thermogenic estrogen-related receptor alpha (23).

Author contributions: H.J.R., A.K.H., S.-I.I., and M.A.L. designed research; H.J.R., A.K.H., S.-I.I., B.N.S., M.K., and M.J.E. performed research; R.N.C. contributed new reagents/analytic tools; H.J.R., K.B., B.N.S., M.J.E., and M.A.L. analyzed data; and H.J.R. and M.A.L. wrote the paper.

Reviewers: C.G., University of California, San Diego; and B.O., Baylor College of Medicine.

Competing interest statement: M.A.L. receives research support from Pfizer for unrelated work, serves as an advisory board member for Pfizer and Flare Therapeutics, is consultant to Madrigal, and holds equity in KDAC Therapeutics and Flare Therapeutics.

[1]To whom correspondence may be addressed. Email: lazar@pennmedicine.upenn.edu.

This article contains supporting information online at http://www.pnas.org/lookup/suppl/doi:10.1073/pnas.2205276119/-/DCSupplemental.

Published August 8, 2022.

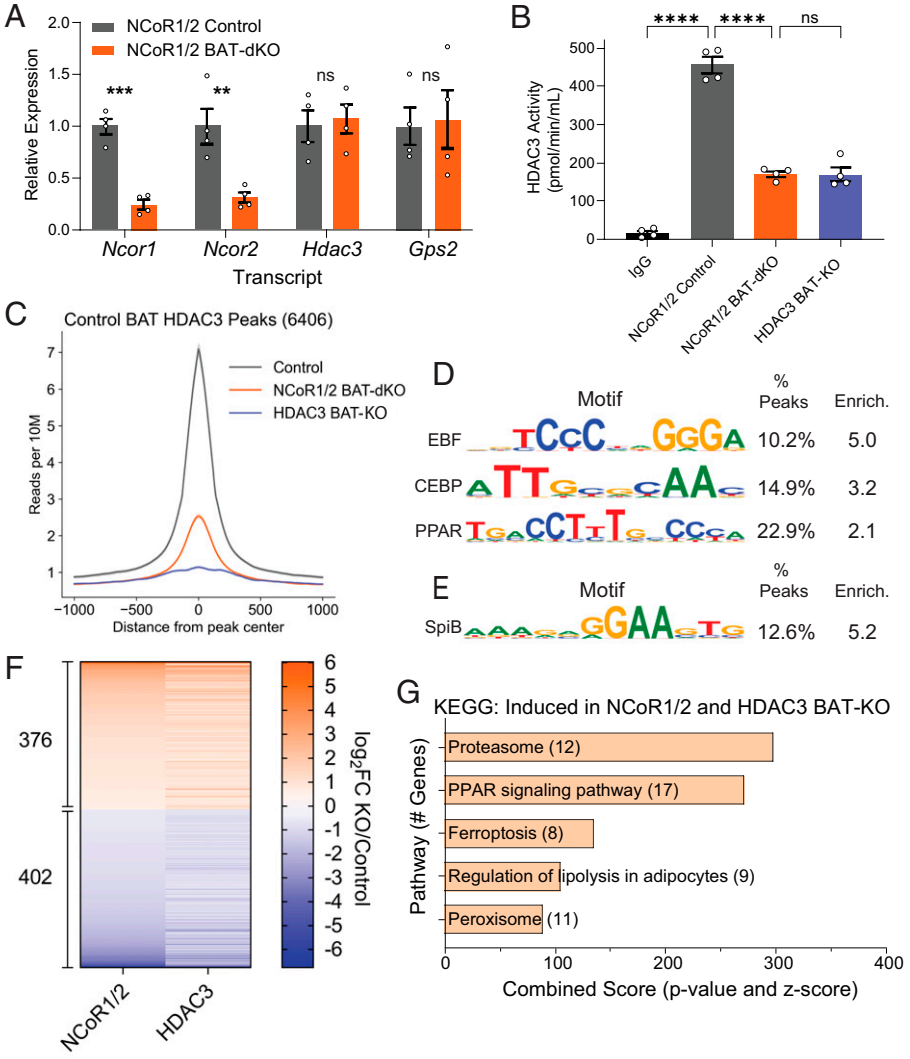

Fig. 1. HDAC3 canonical function and genomic location require NCoR1/2. (*A*) Gene expression in BAT from NCoR1/2 control versus NCoR1/2 BAT-dKO littermates housed at thermoneutrality, normalized to housekeeping transcript and control (n = 4, 4). (*B*) HDAC3 activity in BAT lysates, immunoprecipitated with IgG or HDAC3 antibody (n = 4 per group). (*C*) Average HDAC3 ChIP-seq signal profiles for all HDAC3 peaks (6407) in control BAT. Shaded area: SEM. (*D*) Top enriched known motifs, displaying one example per motif family, using Homer in control HDAC3 peak set. (*E*) Top enriched known motif using Homer in HDAC3 peak set from NCoR1/2 BAT-dKO. (*F*) DEGs shared between NCoR1/2 BAT-dKO and HDAC3 BAT-KO (FC > 1.5 up or down; adjusted $P < 0.05$; n = 3–4 per group). (*G*) KEGG pathways enriched among genes induced in panel *F* highlighting shared regulation of lipid metabolism. ns, not significant.

Because the canonical deacetylase function of HDAC3 requires interaction with NCoR1/2, we hypothesized that depletion of NCoR1/2 in BAT would phenocopy the cold intolerance of mice lacking HDAC3 in BAT. Surprisingly, we found that unlike HDAC3, NCoR1/2 were not required for the acute thermogenic stimulation of BAT, even though HDAC3 genomic binding and activity were dramatically attenuated. In-depth analysis of BAT genes specifically dysregulated in the absence of NCoR1/2 but not HDAC3 revealed the induction of inflammatory pathways, especially IL-17 signaling, which promotes thermogenic innervation of the tissue. Thus, NCoR1/2 regulate inflammation and thermogenesis through mechanisms distinct from HDAC3 in BAT.

Results

Canonical Repressive Role of HDAC3 in BAT Requires NCoR1/2. To study tissue-specific functions of NCoR1 and NCoR2, floxed alleles for both corepressors were crossed with mice transgenic for *Ucp1*-Cre on a C57BL/6J background to knock out (KO) NCoR1/2 in brown adipocytes (24, 25). These alleles allowed efficient depletion of BAT NCoR1/2 protein in the single KOs (sKOs) (*SI Appendix*, Fig. S1*A*). The levels of NCoR1/2 messenger RNA (Fig. 1*A*) were markedly depleted in BAT from the double KO mice (hereafter referred to as NCoR1/2 BAT-dKO mice), with minimal effect on the expression of other key components of the complex, such as HDAC3 and G protein pathway suppressor 2 (GPS2) (Fig. 1*A*). Of note, whereas NCoR1 protein was also diminished in NCoR1/2 BAT-dKO, levels of NCoR2 were similar to those in control mice (*SI Appendix*, Fig. S1*B*). The floxed alleles were deleted as expected (*SI Appendix*, Fig. S1*C*), and therefore, we suspect that the residual protein is in a nonbrown adipocyte cell type specific to dKO. For example, NCoR2 expression is highly enriched in macrophages (26), and as shown below, dKO-BAT is characterized by increased immune cells. Additionally, the enzyme activity of HDAC3 immunoprecipitated from NCoR1/2 BAT-dKO BAT lysates was reduced to an extent indistinguishable from that of HDAC3 in BAT lacking HDAC3 in brown adipocytes (Fig. 1*B*), with remaining activity likely coming from nonadipocytes in the tissue.

We next performed HDAC3 chromatin immunoprecipitation followed by sequencing (ChIP-seq) in BAT from control,

NCoR1/2 BAT-dKO, and HDAC3 BAT-KO animals. This analysis led to the identification of 6,406 high-confidence HDAC3 sites as defined by control signal at least fourfold greater than in HDAC3 BAT-KO (*SI Appendix*, Fig. S1*D*); 85% of these peaks were lost in NCoR1/2 BAT-dKO (*SI Appendix*, Fig. S1*D*), and HDAC3 binding was highly reduced overall (Fig. 1*C*). Motif analysis of control peaks with lost HDAC3 binding in the NCoR1/2 BAT-dKO (Fig. 1*D*) showed high enrichment for transcription factors known to be important for brown adipose lineage, including EBF, C/EBP, and peroxisome proliferator–activated receptors (PPARs) (27). Motif analysis of the HDAC3 peaks remaining in NCoR1/2 BAT-dKO and new HDAC3 binding in NCoR1/2 BAT-dKO revealed enrichment for ETS factors, including SpiB (Fig. 1*E*). These peaks were overall considerably weaker than the HDAC3 peaks in control BAT (*SI Appendix*, Fig. S1*E*) and likely emanated from HDAC3 that remained in nonadipocytic cells, including immune cells in which ETS factors play important roles (28, 29). HDAC3 peaks that were present only in control BAT were near genes enriched for brown adipose and related lineages (*SI Appendix*, Fig. S1*F*), whereas HDAC3 peaks found in NCoR1/2 BAT-dKO were near genes enriched for lung- and immune-related cell types (*SI Appendix*, Fig. S1*G*). Additionally, 491 HDAC3 peaks in NCoR1/2 BAT-dKO tissue overlapped with those in macrophages (30), with high enrichment for the ETS motif of immune cell factor SpiB (*SI Appendix*, Fig. S1*H*), whereas only 71 peaks overlapped between HDAC3 in control BAT and macrophages (*SI Appendix*, Fig. S1*I*). These data are consistent with a model in which the residual and gained HDAC3 peaks in dKO tissue primarily occurred in nonadipocyte cell types in which NCoR1/2 were not deleted.

We next compared the transcriptomes of BAT lacking HDAC3 (23) with those of BAT lacking NCoR1/2 from animals housed at thermoneutrality for 2 wk to remove thermogenic inputs. Using cutoffs of $P < 0.05$ and fold change (FC) > 1.5, 778 unique transcripts were found to be coregulated by HDAC3 and NCoR1/2 (Fig. 1*F*). The up-regulated transcripts were enriched for PPARγ–related lipid-handling pathways (Fig. 1*G*), consistent with the role of the NCoR1/2-HDAC3 complex as a coregulator of PPARγ in adipose tissue as well as the enrichment of the PPARγ binding motif at sites bound by NCoR1/2 and HDAC3 (31, 32). These findings were validated by RT-qPCR for transcripts encoding key lipid metabolism genes (*SI Appendix*, Fig. S1*J*). The shared down-regulated transcripts were not significantly enriched for specific pathways. Together, these data show that NCoR1/2 are required for physiological genomic location and deacetylase function of HDAC3 in BAT, which together regulate lipid metabolism.

Corepressor KO Models Do Not Phenocopy the Cold Intolerance Observed in HDAC3 BAT-KO. Given that NCoR1/2 are required for BAT HDAC3 function at the genome, we next sought to determine if their loss would result in impairment of heat production, as the loss of HDAC3 does in BAT. In agreement with previous studies (23), loss of HDAC3 resulted in marked impairment of norepinephrine-induced thermogenesis, as measured by oxygen consumption in a continuous laboratory animal monitoring system (CLAMS) (Fig. 2*A*). Surprisingly, however, NCoR1/2 BAT-dKO animals displayed no discernable change in thermogenic oxygen consumption compared with control mice (Fig. 2*B*). These animals also did not display any basal changes in metabolic parameters over 72 h of monitoring (*SI Appendix*, Fig. S2). We also tested individual loss of NCoR1 or NCoR2 in BAT to determine whether one but not the other was responsible for the HDAC3 thermogenic phenotype. NCoR1 BAT-sKO mice actually displayed improved thermogenic output (Fig. 2*C*), potentially related to its partnership with circadian nuclear receptor REV-ERBα, which is a negative regulator of BAT thermogenesis (33). However, simultaneous loss of NCoR1 and HDAC3 phenocopied HDAC3 BAT, indicating that the role of HDAC3 was dominant over that of NCoR1 (Fig. 2*D*). Deletion of NCoR2 in BAT had no appreciable effect on thermogenesis (Fig. 2*E*), and the impaired thermogenesis of HDAC3 KO-BAT was retained when NCoR2 was also depleted (Fig. 2*F*). Thus, thermogenesis was impaired by loss of HDAC3 in BAT, and this was not phenocopied by the loss of NCoR1/2, alone or together.

Loss of BAT NCoR1/2 Induces Thermogenic Inflammation. The finding that NCoR1/2 depletion in BAT led to a reduction in HDAC3 enzyme activity and genomic functions but did not phenocopy the physiological effects of HDAC3 loss suggested that additional functions of NCoR1/2 might somehow compensate for or balance the effects of HDAC3 inactivation on thermogenesis. To address this, we focused on the more than 2,000 genes that were differentially expressed in NCoR1/2 dKO-BAT but not HDAC3 KO-BAT (*SI Appendix*, Fig. S3*A*). A total of 1,145 transcripts were up-regulated, matching the canonical repressive function of NCoR1/2, and gene ontology (GO) analysis revealed that this set of genes was highly enriched for immune-related pathways (Fig. 3*A*). Genes related to IL-17 signaling were uniquely enriched in BAT lacking NCoR1/2 (Fig. 3*B*), which was of particular interest because IL-17 signaling via γδT cells has been shown to promote thermogenesis (17, 18) and thus had the potential to offset the thermogenic defect associated with loss of BAT HDAC3.

We next isolated the stromal vascular fraction (SVF) of BAT, which excludes adipocytes and is enriched for immune cells, among other cell types (34). This analysis confirmed that NCoR1/2 were not depleted in nonadipocytic cells of BAT in the KO models (Fig. 3*C*). Moreover, as predicted from the bulk transcriptomics of BAT, γδT-cell genes, such as *Ccl2* and *Il17f*, were up-regulated in these nonadipocytic cells, as were other γδT cell–related genes, including *Cd4* and *Il17a*, whose regulation did not reach significance in bulk transcriptome (Fig. 3*C*). Consistent with this, an increase in immune cells in NCoR/1/2 BAT-dKO was observed by immunohistochemistry (IHC) for CD45, a panhematopoietic marker, and CD68, a monocyte lineage marker (Fig. 3*D*). By contrast, these inflammatory markers were essentially unchanged in HDAC3 BAT-sKO mice (*SI Appendix*, Fig. S3*B*).

IL-17 signaling has been reported to enhance thermogenesis by increasing the sympathetic innervation of BAT, which activates the tissue (17, 35, 36). Immunofluorescence (IF) staining for neuronal markers tyrosine hydroxylase (TH) and Tubulin Beta 3 Class III (Tubb3) revealed a robust increase in the NCoR1/2 BAT-dKO (Fig. 3 *E* and *F*), but not in HDAC3 sKO BAT (*SI Appendix*, Fig. S3 *C* and *D*). Together these data demonstrate that the unique consequence of NCoR1/2 loss in BAT to induce the IL-17 inflammatory axis with an associated increase in thermogenic innervation, which is known to increase thermogenic output.

NCoR1/2 Directly Repress Mmp9, a Key Immune Signaling Factor. Because the increases in immune cells and IL-17 gene expression were likely indirect effects of the specific depletion of NCoR1/2 in brown adipocytes, we next sought to determine

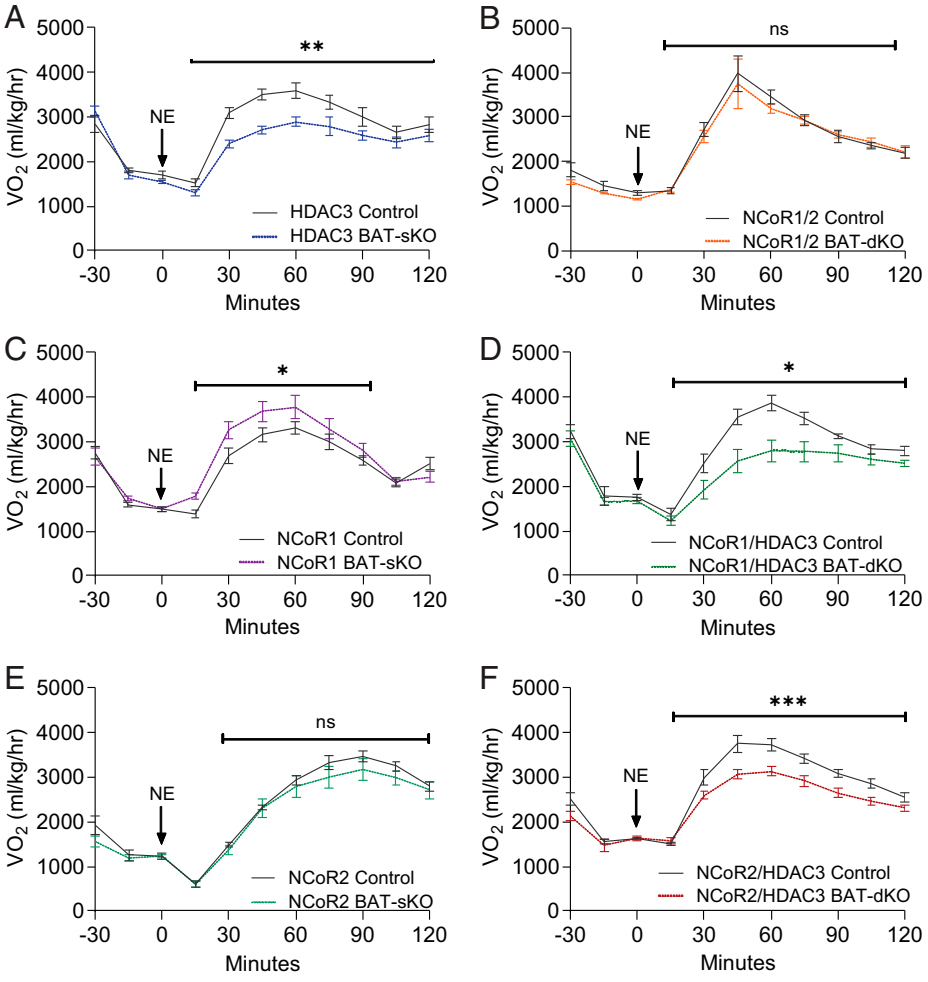

Fig. 2. NCoR1/2 loss does not phenocopy dominant cold intolerance of HDAC3 loss. (*A–F*) Norepinephrine (NE)-induced oxygen consumption following anesthetization at thermoneutrality, after 2 wk of thermoneutral acclimation, for (*A*) NCoR1/2 control versus BAT-dKO (n = 6, 6), (*B*) HDAC3 control versus BAT-sKO (n = 5, 5), (*C*) NCoR1 control versus BAT-sKO (n = 11, 11), (*D*) NCoR1/HDAC3 control versus BAT-dKO (n = 5, 5), (*E*) NCoR2 control versus BAT-sKO (n = 5, 5), and (*F*) NCoR2/HDAC3 control versus BAT-dKO (n = 6, 6). ns, not significant.

the direct transcriptional targets of NCoR1/2 that led to this phenotypic outcome. A total of 525 genes that were transcriptionally up-regulated in NCoR1/2 BAT-dKO, but not NCoR sKO or HDAC3 KO, transcriptomes had a nearby binding peak for NCoR1 in BAT (23) (Fig. 4*A*). These peaks were enriched for NFIL3, NF1, and SpiB binding motifs (*SI Appendix*, Fig. S4*A*) and did not overlap with control HDAC3 peaks (*SI Appendix*, Fig. S4*B*). Analysis of these putative direct NCoR target genes showed that cellular components involved in the extracellular matrix (ECM) were highly enriched (Fig. 4*B*), as was tumor necrosis factor signaling (Fig. 4*C*). By contrast, induction of numerous ECM genes in NCoR1/2 BAT-dKO was not observed in BAT-KO of HDAC3 or NCoR1 or NCoR2 alone (Fig. 4*C*). ECM remodeling, particularly via matrix metalloproteases (Mmps), is known to cause immune cell infiltration into solid tissues and tumors (37). Indeed, *Mmp9* was markedly induced in NCoR1/2 dKO BAT (highlighted in Fig. 4 *D* and *E*). *Mmp9* showed a notable and specific internal NCoR1 binding peak, with little HDAC3 present at the same site (Fig. 4*F*). We also confirmed *Mmp9* up-regulation in NCoR1/2 BAT-dKO and not in HDAC3 BAT-KO by RT-qPCR in a separate cohort, alongside confirmation of other key transcripts (*SI Appendix*, Fig. S4*C*). Thus, the direct effect of NCoR1/2 deletion in brown adipocytes leading to proinflammatory signals was a putative cause of secondary immune infiltration and IL-17 activation in BAT lacking NCoR1/2.

To further confirm the effect of NCoR1/2 deletion on *Mmp9*, primary preadipocytes were harvested from BAT of *Rosa26-CreER* NCoR1/2 floxed animals and control floxed animals. This system displayed good KO efficiency and confirmed direct up-regulation of *Mmp9* in brown adipocytes with loss of NCoR1/2 (Fig. 4*G*). Importantly, loss of NCoR1/2 did not alter adipocytic differentiation, as reflected by gene expression (*SI Appendix*, Fig. S4*D*), or lipid accumulation (*SI Appendix*, Fig. S4*E*). Together, these data suggest that loss of NCoR1/2 in adipocytes directly induced *Mmp9* and potentially other proinflammatory signals that in NCoR1/2 BAT-dKO mice promoted the accumulation and activation of Th17 cells and resulted in increased thermogenic inflammation.

Discussion

Nonshivering thermogenesis is a physiological response to cold that is mediated in part by BAT, with many regulatory mechanisms and inputs to maintain temperature homeostasis and adaptability (5, 38). Here we describe a role for NCoR1/2 in BAT in repressing prothermogenic inflammation via IL-17. This balances the well-established role of NCoR1/2 as obligate activators of the activity of HDAC3 (22, 39), which functions

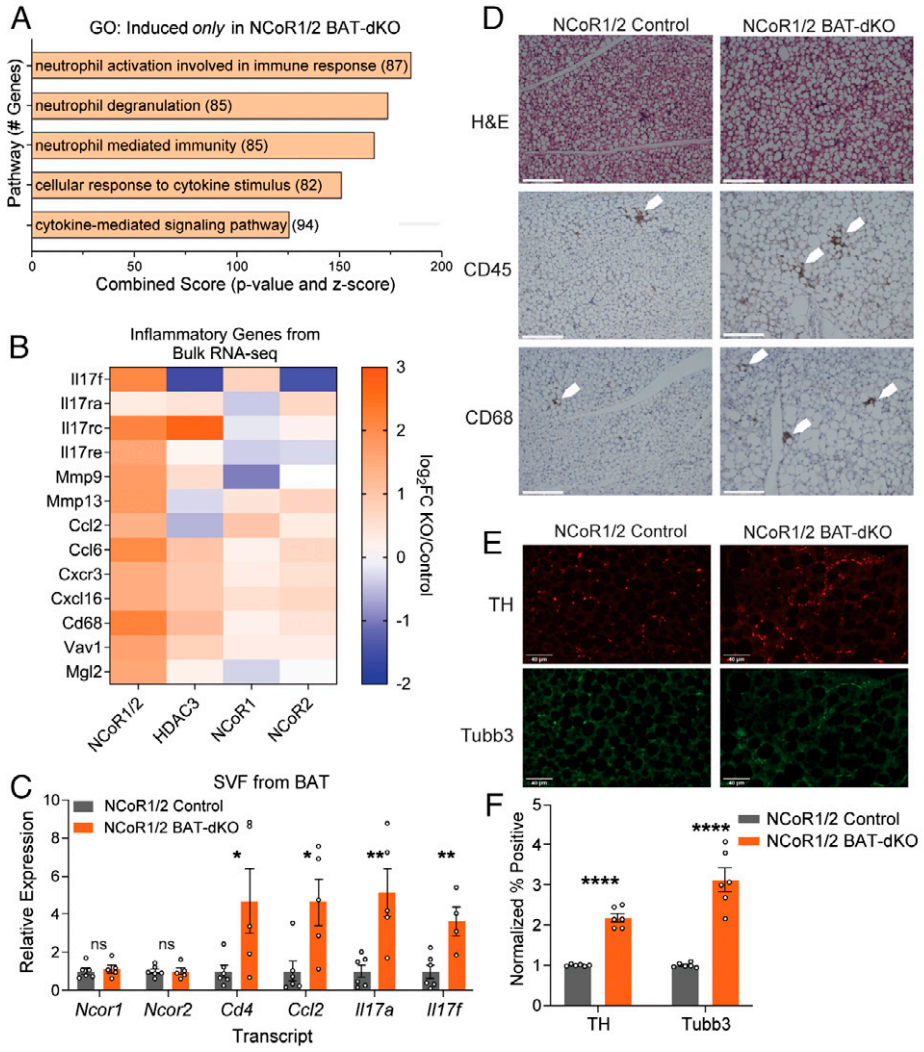

Fig. 3. IL-17 inflammatory axis mediates NCoR1/2 BAT-dKO phenotype. (*A*) GO terms enriched among DEGs induced only in NCoR1/2 BAT-dKO, highlighting inflammatory regulation. (*B*) Heat map of selected inflammatory transcripts related to IL-17 ($n = 3$ per group). (*C*) Gene expression in stromal vascular fraction isolated from BAT of NCoR1/2 control or NCoR1/2 BAT-dKO ($n = 6, 5$). (*D*) Representative images of hematoxylin and eosin (H&E), IHC for CD45, and IHC for CD68 at 20× magnification of BAT from NCoR1/2 control and NCoR1/2 BAT-dKO (scale bar, 200 μM). (*E*) Representative images at 40× magnification of IF for TH and Tubb3 in BAT from NCoR1/2 control and NCoR1/2 BAT-dKO (scale bar, 40 μM). (*F*) Quantification of fluorescent signal in six images per group from two biological replicates stained in parallel, normalized to control.

in BAT as a pilot light required for activation of the coactivator PGC1-α and UCP1 (23) (Fig. 5).

HDAC3, NCoR1, and NCoR2 share the canonical function of repression of sets to genes to which NCoR1/2 get recruited by nuclear receptors and other sequence-specific transcription factors (39). The present findings that NCoR1/2 are required for HDAC3 activity and genomic localization are consistent with these principles, particularly at sites bound by BAT lineage factors, including PPARs, near genes involved in lipid metabolism (29, 31, 40). However, additional levels of complexity have emerged, including functions of HDAC3 that do not require its enzyme activity (41) as well as mechanisms by which HDAC3 may function as a transcriptional coactivator on specific genes (23, 30).

In macrophages, NCoR1/2 are known inflammatory regulators, and there are sets of genes to which HDAC3 is recruited without NCoR1/2 (30, 42). Here we describe functions of NCoR1/2 in brown adipocytes that are distinct from the functions of HDAC3 in these cells. This is perhaps not surprising, because NCoR1/2 are the largest components of a multiprotein repressor complex that also includes TBL1/TBL1R and GPS2 in stoichiometric proportions (37, 43–45). NCoR1/2 bind independently to TBL1/1R (43, 46), and the phenotypes of mice with tissue-specific loss of these components differ in severity and mechanism (47–51), consistent with each component nucleated by NCoR1/2 having separable and sometimes opposing functions. Loss of NCoR1/2 would be expected to result in phenotypes that combine the effects of loss of all of the components and potentially additional NCoR1/2-specific outcomes. Our finding that loss of NCoR1/2, but not HDAC3, in brown adipocytes leads to inflammation of BAT defines one such NCoR1/2-specific function.

The inflammatory response in NCoR1/2 BAT-dKO involves an increase in IL-17 signaling associated with γδT cells. This pathway has recently been shown to increase thermogenesis (17, 18), which could balance the reduction in thermogenesis resulting from loss of HDAC3 (Fig. 5). Different studies have implicated either IL-17A or IL-17F, and indeed, we observed an increase in both γδT-cell cytokines in NCoR1/2-depleted BAT (17, 18). One mechanism by which IL-17 signaling enhances thermogenesis is by increased innervation of BAT (17), which we observed in NCoR1/2 BAT-KO.

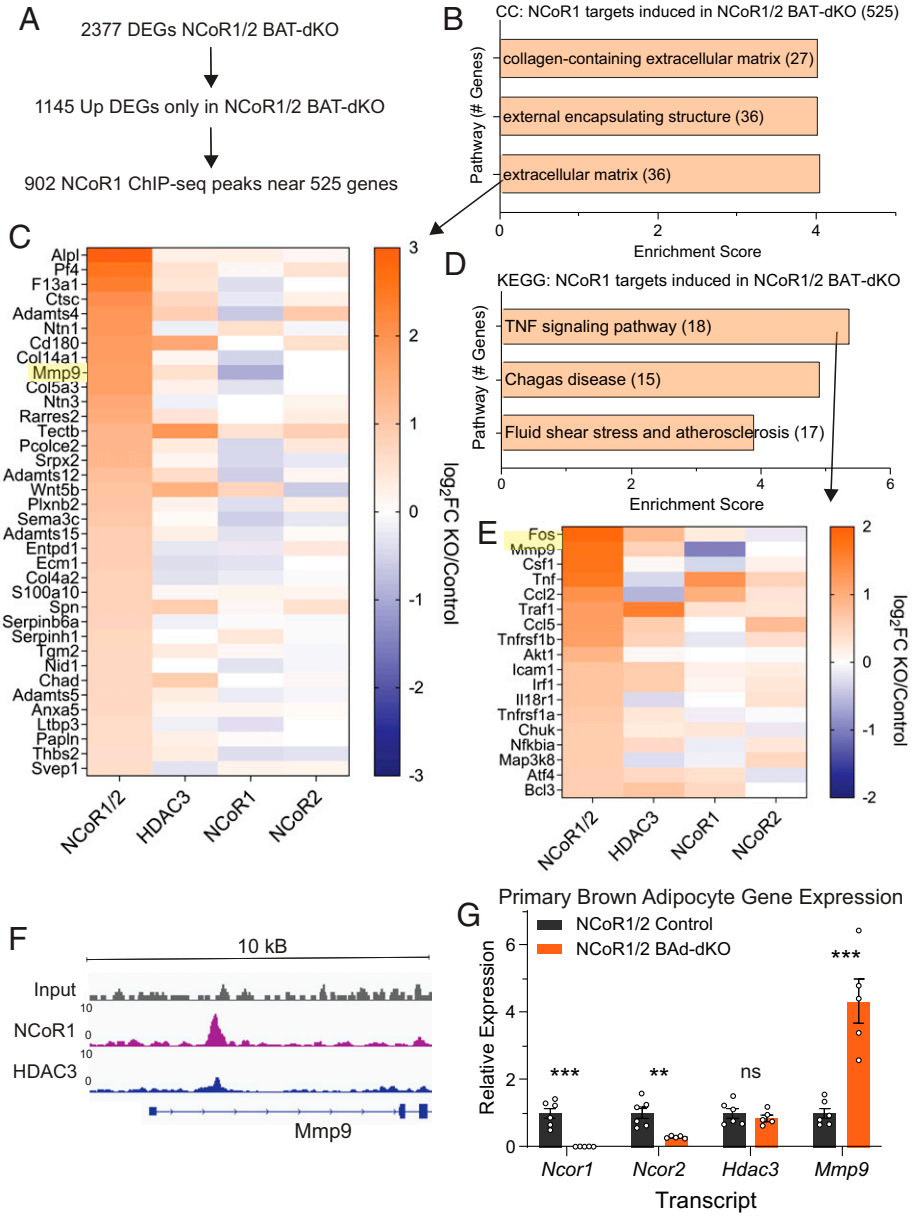

Fig. 4. Brown adipocyte NCoR1/2 together directly regulate Mmp9. (*A*) Schematic of workflow for determining putative direct targets of BAT NCoR1/2. (*B*) Cellular component enrichment for 525 NCoR1/2 BAT target genes found in panel *A*. (*C*) Heat map of extracellular matrix genes regulated by NCoR1/2 in BAT; Mmp9 highlighted. (*D*) KEGG enrichment for 525 NCoR1/2 BAT target genes found in panel *A*. (*E*) Heat map of tumor necrosis factor (TNF) signaling pathway genes regulated by NCoR1/2 in BAT; Mmp9 highlighted. (*F*) Genome browser tracks for NCoR1 and HDAC3 ChIP-seq in BAT at Mmp9 gene locus, with input control shown. (*G*) Gene expression in primary brown adipocytes, either NCoR1/2 control or NCoR1/2 dKO (n = 6, 5).

In this model, NCoR1/2 were deleted in brown adipocytes but not in other cellular components of BAT. As such, the increase in IL-17 signaling was likely an indirect effect of changes in the brown adipocyte. Transcriptomic analysis of the tissue as well as in primary brown adipocytes lacking NCoR1/2 implicated up-regulation of Mmps, which are known to lead to inflammation in cancer (52, 53) as well as in white adipose tissue (54–58). Mmp9, which is increased in obese patients with insulin resistance and sensitive to pioglitazone treatment (59), was markedly induced in BAT lacking NCoR1/2 but not HDAC3. Other factors were also likely to have contributed to the immune infiltration observed in NCoR1/2 BAT-dKO mice. In addition, the exact mechanism by which NCoR1/2 represses *Mmp* and other ECM-related genes, and how this signals to resident inflammatory cells remains to be determined.

Materials and Methods

Animal Husbandry. All animal studies were performed under protocols approved by the University of Pennsylvania Perelman School of Medicine Institutional Animal Care and Use Committee. Mice were group housed in a temperature- and humidity-controlled, specific pathogen-free animal facility at 22 °C under a 12:12-h light–dark cycle with free access to standard chow (LabDiet 5010 postweaning; breeding on LabDiet 5021) and water. Mice were moved to an incubator set to 30 °C 2 wk (14 d) prior to tissue collection or phenotyping unless otherwise noted, with all tissue collection done at ZT10.

NCoR1$^{loxP/loxP}$ mice (strain 033452; The Jackson Laboratory) (24), NCoR2 (SMRT)$^{loxP/loxP}$ (60), and HDAC3$^{loxP/loxP}$ (strain 024119; The Jackson Laboratory) (61) mice were bred to heterozygous *Ucp1*-Cre–expressing mice (strain 024670; The Jackson Laboratory) and maintained on a C57BL/6J background. All BAT-dKO animals were generated by crossing sKO animals in house. All experiments were carried out on 11- to 14-wk-old male littermates generated from *Ucp1*-Cre

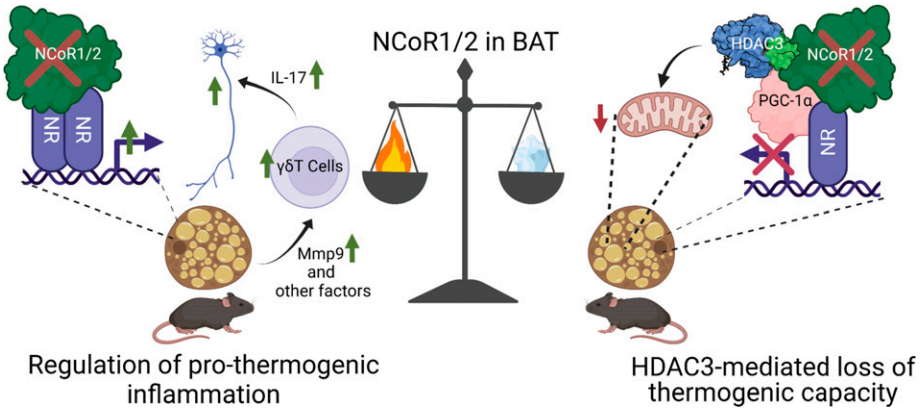

Fig. 5. Integrated model of NCoR1/2 function in BAT. The functions of NCoR1/2 in BAT balance one another to result in a neutral thermogenic state. On one side is the HDAC3-independent prothermogenic inflammatory regulation described in this study, with loss of NCoR1/2 in BAT, which is offset by the loss of thermogenic capacity via HDAC3-mediated PGC1-α deacetylation previously described (23). HDAC3 structure from crystal structure of interaction with NCoR2 (66). NR, nuclear receptor. Created with BioRender.

heterozygous males mated to floxed allele homozygous females, weaned into shared housing.

Isolation and Quantification of RNA (RT-qPCR). RNA was isolated from snap-frozen BAT as previously described (23) using TRIzol-chloroform extraction followed by RNeasy Mini spin columns (Qiagen) and on-column DNase digestion (Qiagen). RNA from cell culture was isolated using the RNeasy Mini Kit protocol (Qiagen). Between 1 and 2 μg total RNA was reverse transcribed to complementary DNA using a HighCapacity cDNA Reverse Transcription Kit (Applied Biosystems). RT-qPCR was performed using standard curve-based normalization and Power SYBR Green PCR Master Mix on the Quant Studio 6 Flex Real-Time PCR System (Applied Biosystems), with all transcripts further normalized to *18s* quantity and average expression in the control group. Biological replicates are shown in bar graphs. The primer table (*SI Appendix*, Table S1) provides for specific primer sequences.

HDAC3 Activity. HDAC3 activity was assayed using the HDAC3 Activity Assay Kit (EPI004; Sigma-Aldrich). Protein lysates were quantified by BCA and normalized to 2 μg total starting material. Material was then incubated overnight with HDAC3 antibody (85057S; Cell Signaling Technology) or rabbit immunoglobulin G (IgG) (2729S; Cell Signaling Technology) and immunoprecipitated with protein A DynaBeads (10002D; Invitrogen). Assay incubations were performed on bead with final sample removed from beads for measurement and normalization according to kit instructions.

ChIP. ChIP was performed as previously described, with minor modifications (23). Total protein for each sonicated sample was quantified by bicinchoninic acid (BCA) and normalized to 1.5 μg protein for each ChIP prior to incubation with antibody overnight; 5% input was saved prior to antibody incubation and used as input control. Antibodies used were HDAC3 (GTX109679; Genetex) and rabbit IgG (2729S; Cell Signaling Technology) and immunoprecipitated with bovine serum albumin (BSA)–blocked protein A agarose beads (15918014; Invitrogen). ChIP DNA was isolated using phenol/chloroform extraction and treated with RNase A prior to sequencing library preparation.

ChIP-seq Preparation and Analysis. The NEBNext Ultra II DNA Library Prep Kit for Illumina (E7645S; New England BioLabs) with AMPure XP Beads (A63881; Beckman Coulter, Inc.) was used to amplify and size select ChIP DNA. The Agilent High Sensitivity DNA Kit (5007-4626) and KAPA Library Quantification Kit (KR0405) were used to quantify libraries and fragment sizes prior to sequencing. $n = 3$ was sequenced for NCoR1/2 control and NCoR1/2 BAT-dKO groups, $n = 2$ for HDAC3 BAT-KO, and $n = 1$ each for input and IgG. The sequencing was performed at the Next-Generation Sequencing Core at the University of Pennsylvania on a NextSeq platform (Illumina) at 100SR for a total of 30 million reads per sample.

FASTQ files were aligned to the GRCm38 (mm10) reference genome using the bowtie2 v2.4.2 aligner with the following parameters: -N 1. Duplicate reads were removed with samtools rmdup. Tag directories were then made with Homer v4.11.1. HDAC3 peaks in control and NCoR1/2 dKO were called using Homer from pooled replicates, using HDAC3 KO as background. findPeaks was used with default parameters, which sets the cutoff to fourfold minimum enrichment over the background. Homer's mergePeaks was used to intersect the two peak sets and determine control-only, NCoR1/2-only, and shared peaks. Motif enrichment analysis in various peak sets was performed with Homer's findMotifsGenome.pl with the following parameters: -size 200 -S 10 -len 8,10,12,14,16. Enrichment score for a motif was calculated as the fraction of target peaks having the motif divided by the fraction of background regions containing the motif. Genes nearest to the peaks were found with Homer's annotatePeaks.pl.

RNA-Seq Preparation and Analysis. We analyzed an n of 4 for each group: NCoR2 control, NCoR2 BAT-sKO, NCoR1/2 control, and NCoR1/2 BAT-dKO. Isolated RNA from these groups was sequenced at Novogene using an Illumina Platform PE150, with ∼30 million reads per sample. For NCoR1 control ($n = 4$) and NCoR1 BAT-sKO ($n = 3$), libraries were prepared using the TruSeq Stranded Total RNA Kit (Illumina) and sequenced at the Next-Generation Sequencing Core at the University of Pennsylvania on the NextSeq 500 platform (Illumina) at 75SR for a total of 20 to 40 million reads per sample.

RNA-seq output, including published HDAC3 BAT-KO data (23), was analyzed in tandem using the DIYTranscriptomics course pipeline (62). Briefly, this pipeline uses Kallisto to align and quantify reads, EnemblDB to annotate data, edgeR to normalize read counts, and Limma to determine differentially expressed genes (DEGs). Cutoffs used for these analyses were a CPM of 1 in a minimum of 4 of 31 total samples to identify a transcript as expressed and a $\log_2$FC $> |0.58|$ and adjusted P value <0.05 for all DEGs per mouse line. GO analysis for RNA-seq was performed using Enrichr (63), with the top ranked KEGG or GO pathways selected by Enrichr combined score. All heat maps are presented as $\log_2$FC for KO over control per mouse line and were generated in GraphPad PRISM 9.3.1 using output files from the above pipeline.

Western Blot. Whole-tissue BAT lysates were prepared as previously described and quantified by Direct Detect (Millipore) (23). For blotting NCoR1/2, 50 μg protein lysate was loaded per lane, with each lane representing a separate biological replicate. Ladder used was a prestained high-range multicolor protein ladder (26625; Thermo Fisher Scientific). Wet transfer to PVDF was done overnight, and primary antibodies were applied in 5% BSA overnight, all at 4 °C. Primary antibodies used were anti-SMRTe (06-891; Millipore; 1:1,000), anti-NCoR1 (5948S; Cell Signaling Technology; 1:1,000), and anti-Vinculin (V9264; Sigma; 1:5,000), with appropriate HRP-linked secondary antibodies (Cell Signaling Technology; 1:10,000) applied at room temperature for 1 h. Blots were revealed using either film or a Bio-Rad ChemiDoc.

Metabolic Phenotyping and Norepinephrine Response. All metabolic phenotyping data were collected using CLAMS (Columbus Instruments) metabolic cages housed within environment-controlled incubators. Norepinephrine response was measured as previously described (23). Briefly, oxygen consumption was

measured prior to and for 2 h following subcutaneous injection of 1 mg kg^{-1} L-(−)-Norepinephrine (+)-bitartrate salt monohydrate (A9512; Sigma) dissolved in sterile 0.9% NaCl above BAT in anesthetized animals.

Histology. Freshly isolated tissue was fixed overnight in 4% paraformaldehyde at 4 °C and dehydrated prior to embedding in paraffin and sectioning at a thickness of 7 μm. Slides were prepared with two replicates each for control and KO on a single slide for even processing. Hematoxylin and eosin stain was applied by the Institute for Diabetes, Obesity, and Metabolism Histology Core using a standard protocol.

IHC. IHC for CD45 (208022; Abcam) and CD68 (283654; Abcam) was performed using a standard IHC protocol. Dilutions used were 1:800 for CD45 and 1:400 for CD68. High pH antigen retrieval solution (00-4956-58; Invitrogen) was applied prior to CD68 staining. Simple Stain Mouse MAX PO (NIC-414142F; Cosmo Bio) was used as a secondary stain and revealed with DAB. Slides were then counterstained with Carazzi hematoxylin before mounting in Cytoseal XYL (8312-4; Thermo Fisher Scientific). Slides were imaged on a ThermoFisher EVOS FL Auto 2 at 20× magnification, choosing representative areas from 4× imaging.

Immunofluorescence. Immunofluorescence for Tubb3 (52623; Abcam) and TH (AB1542; EMD Millipore) was performed as previously described (17). Dilutions used were 1:200 for TH and 1:800 for Tubb3, with 1:500 used for secondary antibodies. Sections were mounted with DAPI Fluoromount (0100-20; SouthernBiotech) and imaged using a Zeiss Observer 7 at 40× magnification. Fluorescent signal in each image layer was quantified using Fiji automatic signal measurement prior to any adjustment of image brightness or contrast and normalized to the average of the control signal (64). The final resolution of the 40× images was 1,920 × 1,210 with a pixel width of 0.1465 microns.

BAT Fractionation. For SVF isolation, BAT was harvested from adult mice and incubated in a gentleMACS Dissociator (130-096-427; Miltenyi Biotech) with 2.4 U/mL Dispase II and 1.5 U/mL type I collagenase for 40 min at 37 °C. Lysate was then filtered over a 200-μM filter before a gentle spin for 3 min at 50 *g*. The adipocyte layer was carefully removed from the top of the lysate before a second spin for 5 min at 500 *g* to pellet SVF. Pelleted SVF was then resuspended in TRIzol for RNA isolation and quantification.

Primary Brown Adipocyte Culture. Primary brown preadipocytes were isolated and differentiated in culture as previously described from BAT of 1- to 5-d-old pups (23). Genotype of pups was either *Rosa26-CreER* positive or negative and all NCoR1/2 floxed. Isolated cells were initially pooled by genotype and tamoxifen applied to all wells from days 0 to 2 of differentiation. Replicates were differentiated individually in 12-well plates prior to isolation of RNA as described in Isolation and Quantification of RNA (RT-qPCR). Oil Red O staining was performed as previously described (65) to confirm differentiation in separate six-well plates and imaged at 20× on a ThermoFisher EVOS FL Auto 2 microscope.

Statistical Analysis. Statistical analyses were performed using R (version 4.1) for sequencing data (as described in the sequencing analyses sections) and GraphPad Prism (version 9.3) for all other data types. All data with error bars are presented as mean ± SEM with replicates shown as individual points. Statistical analyses used were unpaired two-tailed *t* tests for direct comparisons between two groups, two-way ANOVAs with repeated measures for analysis of two groups over time, or one-way ANOVA with Tukey corrected multiple comparisons for analysis of a single variable between multiple groups. *P* values throughout are reported as $*P < 0.05$, $**P < 0.01$, $***P < 0.001$, and $****P < 0.0001$, with adjusted *P* values used where appropriate.

Data Availability. RNA-seq and ChIP-seq data have been deposited in Gene Expression Omnibus (accession number GSE199808 (67)).

ACKNOWLEDGMENTS. We thank C. D. Holman and C. C. Chan for valuable discussions and B. J. Carpenter and B. M. Krusen for assistance with animal husbandry. We are grateful to L. Chang of the Histology Core of the Institute for Diabetes, Obesity, and Metabolism for slide preparation and to J. Zhao of the Cell and Developmental Biology Microscopy Core for microscopy training and assistance. We also thank the Functional Genomics Core and Rodent Metabolic Phenotyping Core of the Penn Diabetes Center (DK19525) for next-generation sequencing and CLAMS experiments, respectively. Next-generation sequencing data are available at Gene Expression Omnibus accession number GSE199808. This work was supported by National Institutes of Health (NIH) grant R01 DK43806 (M.A.L.), NIH grants T32 DK007314 and F32 DK122684 (A.K.H.), the Uehara Memorial Foundation, the Leading Young Researcher Overseas Visit Program and the Osamu Hayaishi Memorial Scholarship for Study Abroad (S.-I.I.), the Cox Medical Research Institute, and the JPB Foundation.

Author affiliations: [a]Biochemistry and Molecular Biophysics Graduate Group, University of Pennsylvania Perelman School of Medicine, Philadelphia, PA 19104; [b]Institute for Diabetes, Obesity, and Metabolism, University of Pennsylvania Perelman School of Medicine, Philadelphia, PA 19104; [c]Division of Endocrinology, Diabetes, and Metabolism, Department of Medicine, University of Pennsylvania Perelman School of Medicine, Philadelphia, PA 19104; and [d]Section of Endocrinology, Diabetes, and Metabolism, University of Chicago, Chicago, IL 60637

1. Y. Wang *et al.*, Has the prevalence of overweight, obesity and central obesity levelled off in the United States? Trends, patterns, disparities, and future projections for the obesity epidemic. *Int. J. Epidemiol.* **49**, 810–823 (2020).
2. A. Ruban, K. Stoenchev, H. Ashrafian, J. Teare, Current treatments for obesity. *Clin. Med. (Lond.)* **19**, 205–212 (2019).
3. L. Cheng *et al.*, Brown and beige adipose tissue: A novel therapeutic strategy for obesity and type 2 diabetes mellitus. *Adipocyte* **10**, 48–65 (2021).
4. C.-H. Wang, Y.-H. Wei, Therapeutic perspectives of thermogenic adipocytes in obesity and related complications. *Int. J. Mol. Sci.* **22**, 7177 (2021).
5. B. Cannon, J. Nedergaard, Brown adipose tissue: Function and physiological significance. *Physiol. Rev.* **84**, 277–359 (2004).
6. A. M. Cypess *et al.*, Activation of human brown adipose tissue by a β3-adrenergic receptor agonist. *Cell Metab.* **21**, 33–38 (2015).
7. K. L. Townsend, Y.-H. Tseng, Brown fat fuel utilization and thermogenesis. *Trends Endocrinol. Metab.* **25**, 168–177 (2014).
8. E. T. Chouchani, L. Kazak, B. M. Spiegelman, New advances in adaptive thermogenesis: UCP1 and beyond. *Cell Metab.* **29**, 27–37 (2019).
9. F. Omran, M. Christian, Inflammatory signaling and brown fat activity. *Front. Endocrinol.* **11**, 156 (2020).
10. D. A. Hill *et al.*, Distinct macrophage populations direct inflammatory versus physiological changes in adipose tissue. *Proc. Natl. Acad. Sci. U.S.A.* **115**, E5096–E5105 (2018).
11. H. L. Caslin, M. Bhanot, W. R. Bolus, A. H. Hasty, Adipose tissue macrophages: Unique polarization and bioenergetics in obesity. *Immunol. Rev.* **295**, 101–113 (2020).
12. S. M. Reilly, A. R. Saltiel, Adapting to obesity with adipose tissue inflammation. *Nat. Rev. Endocrinol.* **13**, 633–643 (2017).
13. F. Villarroya, R. Cereijo, A. Gavaldà-Navarro, J. Villarroya, M. Giralt, Inflammation of brown/beige adipose tissues in obesity and metabolic disease. *J. Intern. Med.* **284**, 492–504 (2018).
14. K. Fischer *et al.*, Alternatively activated macrophages do not synthesize catecholamines or contribute to adipose tissue adaptive thermogenesis. *Nat. Med.* **23**, 623–630 (2017).
15. M.-W. Lee *et al.*, Activated type 2 innate lymphoid cells regulate beige fat biogenesis. *Cell* **160**, 74–87 (2015).
16. K. D. Nguyen *et al.*, Alternatively activated macrophages produce catecholamines to sustain adaptive thermogenesis. *Nature* **480**, 104–108 (2011).
17. B. Hu *et al.*, γδ T cells and adipocyte IL-17RC control fat innervation and thermogenesis. *Nature* **578**, 610–614 (2020).
18. A. C. Kohlgruber *et al.*, γδ T cells producing interleukin-17A regulate adipose regulatory T cell homeostasis and thermogenesis. *Nat. Immunol.* **19**, 464–474 (2018).
19. C. K. Glass, M. G. Rosenfeld, The coregulator exchange in transcriptional functions of nuclear receptors. *Genes Dev.* **14**, 121–141 (2000).
20. D. M. Lonard, B. W. O'Malley, Nuclear receptor coregulators: Modulators of pathology and therapeutic targets. *Nat. Rev. Endocrinol.* **8**, 598–604 (2012).
21. N. Liang, T. Jakobsson, R. Fan, E. Treuter, The nuclear receptor-co-repressor complex in control of liver metabolism and disease. *Front. Endocrinol. (Lausanne)* **10**, 411 (2019).
22. M. G. Guenther, O. Barak, M. A. Lazar, The SMRT and N-CoR corepressors are activating cofactors for histone deacetylase 3. *Mol. Cell. Biol.* **21**, 6091–6101 (2001).
23. M. J. Emmett *et al.*, Histone deacetylase 3 prepares brown adipose tissue for acute thermogenic challenge. *Nature* **546**, 544–548 (2017).
24. H. Yamamoto *et al.*, NCoR1 is a conserved physiological modulator of muscle mass and oxidative function. *Cell* **147**, 827–839 (2011).
25. J. H. Kahn *et al.*, SMRT regulates metabolic homeostasis and adipose tissue macrophage phenotypes in tandem. *Endocrinology* **161**, bqaa132 (2020).
26. W. Sun *et al.*, snRNA-seq reveals a subpopulation of adipocytes that regulates thermogenesis. *Nature* **587**, 98–102 (2020).
27. T. Inagaki, J. Sakai, S. Kajimura, Transcriptional and epigenetic control of brown and beige adipose cell fate and function. *Nat. Rev. Mol. Cell Biol.* **17**, 480–495 (2016).
28. A.-S. Laramée *et al.*, Opposing roles for the related ETS-family transcription factors Spi-B and Spi-C in regulating B cell differentiation and function. *Front. Immunol.* **11**, 841 (2020).
29. A. G. Bassuk, J. M. Leiden, "The role of Ets transcription factors in the development and function of the mammalian immune system" in *Advances in Immunology*, F. J. Dixon, Ed. (Academic Press, Cambridge, Massachusetts, 1997), pp. 65–104.
30. H. C. B. Nguyen, M. Adlanmerini, A. K. Hauck, M. A. Lazar, Dichotomous engagement of HDAC3 activity governs inflammatory responses. *Nature* **584**, 286–290 (2020).

31. C. Yu *et al.*, The nuclear receptor corepressors NCoR and SMRT decrease peroxisome proliferator-activated receptor γ transcriptional activity and repress 3T3-L1 adipogenesis. *J. Biol. Chem.* **280**, 13600–13605 (2005).
32. P. Li *et al.*, Adipocyte NCoR knockout decreases PPARγ phosphorylation and enhances PPARγ activity and insulin sensitivity. *Cell* **147**, 815–826 (2011).
33. Z. Gerhart-Hines *et al.*, The nuclear receptor Rev-erbα controls circadian thermogenic plasticity. *Nature* **503**, 410–413 (2013).
34. V. M. Ramakrishnan, N. L. Boyd, The adipose stromal vascular fraction as a complex cellular source for tissue engineering applications. *Tissue Eng. Part B Rev.* **24**, 289–299 (2018).
35. M. François *et al.*, Sympathetic innervation of the interscapular brown adipose tissue in mouse. *Ann. N. Y. Acad. Sci.* **1454**, 3–13 (2019).
36. T. J. Bartness, C. H. Vaughan, C. K. Song, Sympathetic and sensory innervation of brown adipose tissue. *Int. J. Obes.* **34** (suppl. 1), S36–S42 (2010).
37. R. Watanabe *et al.*, MMP (matrix metalloprotease)-9-producing monocytes enable T cells to invade the vessel wall and cause vasculitis. *Circ. Res.* **123**, 700–715 (2018).
38. Z. Zhang *et al.*, Non-shivering thermogenesis signalling regulation and potential therapeutic applications of brown adipose tissue. *Int. J. Biol. Sci.* **17**, 2853–2870 (2021).
39. J. Zhang, M. Kalkum, B. T. Chait, R. G. Roeder, The N-CoR-HDAC3 nuclear receptor corepressor complex inhibits the JNK pathway through the integral subunit GPS2. *Mol. Cell* **9**, 611–623 (2002).
40. M. J. Emmett, M. A. Lazar, Integrative regulation of physiology by histone deacetylase 3. *Nat. Rev. Mol. Cell Biol.* **20**, 102–115 (2019).
41. Z. Sun *et al.*, Deacetylase-independent function of HDAC3 in transcription and metabolism requires nuclear receptor corepressor. *Mol. Cell* **52**, 769–782 (2013).
42. S. Ghisletti *et al.*, Cooperative NCoR/SMRT interactions establish a corepressor-based strategy for integration of inflammatory and anti-inflammatory signaling pathways. *Genes Dev.* **23**, 681–693 (2009).
43. M. G. Guenther, M. A. Lazar, Biochemical isolation and analysis of a nuclear receptor corepressor complex. *Methods Enzymology.* **364**, 246–257 (2003).
44. Y.-D. Wen *et al.*, The histone deacetylase-3 complex contains nuclear receptor corepressors. *Proc. Natl. Acad. Sci. U.S.A.* **97**, 7202–7207 (2000).
45. E. Y. Huang *et al.*, Nuclear receptor corepressors partner with class II histone deacetylases in a Sin3-independent repression pathway. *Genes Dev.* **14**, 45–54 (2000).
46. A. Codina *et al.*, Structural insights into the interaction and activation of histone deacetylase 3 by nuclear receptor corepressors. *Proc. Natl. Acad. Sci. U.S.A.* **102**, 6009–6014 (2005).
47. P. Kulozik *et al.*, Hepatic deficiency in transcriptional cofactor TBL1 promotes liver steatosis and hypertriglyceridemia. *Cell Metab.* **13**, 389–400 (2011).
48. N. Liang *et al.*, Hepatocyte-specific loss of GPS2 in mice reduces non-alcoholic steatohepatitis via activation of PPARα. *Nat. Commun.* **10**, 1684 (2019).
49. C. T. Cederquist *et al.*, Systemic insulin sensitivity is regulated by GPS2 inhibition of AKT ubiquitination and activation in adipose tissue. *Mol. Metab.* **6**, 125–137 (2016).
50. Z. Sun *et al.*, Hepatic Hdac3 promotes gluconeogenesis by repressing lipid synthesis and sequestration. *Nat. Med.* **18**, 934–942 (2012).
51. V. Perissi *et al.*, TBL1 and TBLR1 phosphorylation on regulated gene promoters overcomes dual CtBP and NCoR/SMRT transcriptional repression checkpoints. *Mol. Cell* **29**, 755–766 (2008).
52. S. Löffek, O. Schilling, C.-W. Franzke, Series "matrix metalloproteinases in lung health and disease": Biological role of matrix metalloproteinases: A critical balance. *Eur. Respir. J.* **38**, 191–208 (2011).
53. K. Kessenbrock, V. Plaks, Z. Werb, Matrix metalloproteinases: Regulators of the tumor microenvironment. *Cell* **141**, 52–67 (2010).
54. F. J. Ruiz-Ojeda, A. Méndez-Gutiérrez, C. M. Aguilera, J. Plaza-Díaz, Extracellular matrix remodeling of adipose tissue in obesity and metabolic diseases. *Int. J. Mol. Sci.* **20**, 4888 (2019).
55. C. Strieder-Barboza *et al.*, Depot-specific adipocyte-extracellular matrix metabolic crosstalk in murine obesity. *Adipocyte* **9**, 189–196 (2020).
56. M. A. Gonzalez Porras *et al.*, Integrins and extracellular matrix proteins modulate adipocyte thermogenic capacity. *Sci. Rep.* **11**, 5442 (2021).
57. G. Berg, M. Barchuk, V. Miksztowicz, Behavior of metalloproteinases in adipose tissue, liver and arterial wall: An update of extracellular matrix remodeling. *Cells* **8**, 158 (2019).
58. T.-H. Chun *et al.*, Genetic link between obesity and MMP14-dependent adipogenic collagen turnover. *Diabetes* **59**, 2484–2494 (2010).
59. R. Unal *et al.*, Matrix metalloproteinase-9 is increased in obese subjects and decreases in response to pioglitazone. *J. Clin. Endocrinol. Metab.* **95**, 2993–3001 (2010).
60. H. Shimizu *et al.*, NCoR1 and SMRT play unique roles in thyroid hormone action in vivo. *Mol. Cell. Biol.* **35**, 555–565 (2015).
61. S. E. Mullican *et al.*, Histone deacetylase 3 is an epigenomic brake in macrophage alternative activation. *Genes Dev.* **25**, 2480–2488 (2011).
62. A. S. F. Berry *et al.*, An open-source toolkit to expand bioinformatics training in infectious diseases. *mBio* **12**, e0121421 (2021).
63. Z. Xie *et al.*, Gene set knowledge discovery with enrichr. *Curr. Protoc.* **1**, e90 (2021).
64. J. Schindelin *et al.*, Fiji: An open-source platform for biological-image analysis. *Nat. Methods* **9**, 676–682 (2012).
65. W. Wang *et al.*, Ebf2 is a selective marker of brown and beige adipogenic precursor cells. *Proc. Natl. Acad. Sci. U.S.A.* **111**, 14466–14471 (2014).
66. P. J. Watson, L. Fairall, G. M. Santos, J. W. R. Schwabe, Structure of HDAC3 bound to co-repressor and inositol tetraphosphate. *Nature* **481**, 335–340 (2012).
67. H. J. Richter *et al.*, Balanced Control of Thermogenesis by Nuclear Receptor Corepressors in Brown Adipose Tissue. NCBI GEO. https://www.ncbi.nlm.nih.gov/geo/query/acc.cgi?acc=GSE199808. Deposited 30 March 2022.